Pressure–volume–temperature paths in the laser-heated diamond anvil cell

Abby Kavner[a)] and Thomas S. Duffy

Department of Geosciences, Princeton University, Princeton, New Jersey 08544

The temperature, pressure, and stress conditions in the diamond anvil cell sample chamber before, during, and after laser heating are mapped by employing standard materials as *in situ* pressure markers. Unit cell volumes of Pt, MgO, and NaCl were monitored by synchrotron-based x-ray diffraction at temperatures between 300 and 2290 K and pressures ranging from 14 to 53 GPa. To aid in interpreting the resulting pressure–volume–temperature paths, we perform a series of model calculations of the high-temperature, high-pressure x-ray diffraction behavior of platinum subjected to a general stress state. Thermal pressure and thermal expansion effects within the laser-heated volume are observed but are not sufficient to fully explain the measured paths. Large apparent pressure changes can also result from relaxation of deviatoric stresses during heating and partial reintroduction of those stresses during quench. Deviatoric stresses, monitored from both diffraction peak widths and lattice parameter shifts as a function of (hkl), may significantly distort equation of state results if it is assumed that the sample is under hydrostatic pressure. Large-scale, nearly isothermal pressure relaxation events are observed at $\sim$2000 K. It is proposed that these arise from relaxation of heated components (pressure medium, gasket, cell itself) outside of the directly laser-heated volume. © *2001 American Institute of Physics.* [DOI: 10.1063/1.1335827]

INTRODUCTION

The ability to measure the behavior of Earth and planetary materials at extreme conditions of pressure and temperature is of fundamental importance to interpreting seismologic, geodynamic, and geodesic models of planetary interiors. Due to its ability to access nearly the entire range of pressure and temperature conditions of terrestrial planetary interiors, the laser-heated diamond anvil cell is an important tool for measuring high-pressure, high-temperature thermoelastic properties. Obtaining sufficiently precise and accurate quantities requires that the pressure and temperature are well characterized and controlled. This article focuses on determining the evolution of the stress distribution within the sample chamber of a diamond cell as it is laser heated to geologically relevant temperatures. Such characterization is a crucial step toward realizing the goal of accurate determination of thermoelastic properties under these conditions.

The experiment to measure the high-temperature equation of state of a material in the diamond cell is simple in concept. A material of interest is loaded within the gasketted sample chamber and insulated from the diamonds. Ideally, the stress state within the sample chamber is hydrostatic, and the pressure is measured either by ruby fluorescence[1] or by measuring the unit cell volume (from x-ray diffraction lines) of a previously calibrated standard material.[2] High temperatures are generated by laser heating and measured by spectroradiometry.[3] The volume of the sample is measured by powder x-ray diffraction techniques as a function of temperature during a heating cycle at constant pressure (Fig. 1, path a), and the experiment is repeated at different pressures

to yield the complete pressure (volume, temperature) $[P(V,T)]$ equation of state.

However, this ideal experiment cannot be achieved in practice due to several interrelated factors. If the sample volume is constrained during heating, there is a pressure increase up to the maximum value allowed by the thermal pressure, $P_{th}=(\partial P/\partial T)_v$[4–7] (Fig. 1, path b). This picture is further complicated by the fact that the stress state within the diamond cell at low temperatures may not be hydrostatic.[8–10] The presence of deviatoric stresses may affect the pressure determination when using an x-ray standard. Available data from the diamond anvil cell[11] and the large volume press[12,13] indicate that deviatoric stresses decrease rapidly at high temperature but detailed understanding of material strength at high pressures and temperatures is limited. In addition, there is also evidence that temperature quenched laser-heated samples can exhibit considerable shear stresses.[14] A third difficulty is that there are few x-ray standards whose high pressure–temperature equations of state have been determined and their accuracy is not well known.[2,12] Finally, there are significant difficulties in temperature measurement, primarily arising from difficulty in controlling and measuring the steep temperature gradients generated within the sample during these experiments.[15–18]

Fully understanding the evolution of the stress state in the laser-heated diamond cell has been recognized as a potentially key parameter in resolving conflicting experimental results regarding phase boundaries of fundamental importance to the deep Earth such as the stability of $MgSiO_3$ pervoskite[19–22] and the coesite–stishovite transformation in SiO_2.[6,23–26] It is also recognized as essential for accurate $P(V,T)$ equation of state determination.[4,26,27] Here we examine the stress state evolution inside the sample chamber during heating by examining the high $P–T$ behavior of standard

[a)]Present address: Lamont Doherty Earth Observatory, 61 Rt. 9W, Palisades, NY 10964; electronic mail: KAVNER@LDEO.COLUMBIA.EDU
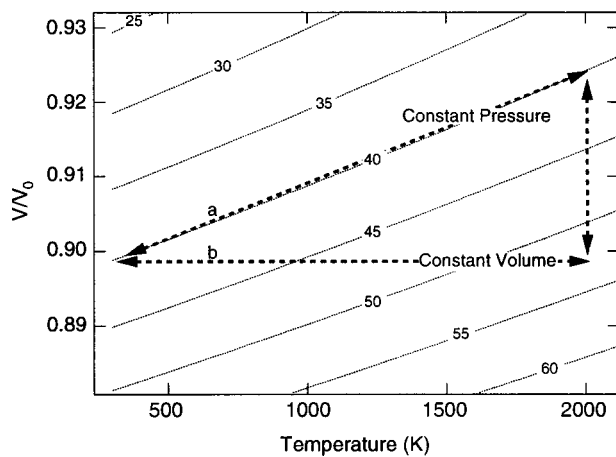
FIG. 1. Volume compression as a function of temperature for platinum. Constant pressure and constant volume heating and cooling paths are delineated with dashed lines. Contours show corresponding pressures (in GPa) obtained from equation of state parameters (Table II).

materials by synchrotron x-ray diffraction during laser heating within the diamond anvil cell. The standards—platinum, MgO, and NaCl—were chosen on one or more of the following grounds: ability to couple with the laser for heating, relative lack of reactivity, cubic structures with wide $P-T$ stability, and relatively well-characterized high pressure–temperature equations of state.

EXPERIMENTAL PROCEDURE

Samples were prepared by mixing <1 μm platinum powder (99.9%, Aldrich Chem. Co.) with either MgO or NaCl powder in a ratio of 1:6 by weight, and compressing the mixture into ~10 μm thick foils. The sample was then loaded into a stainless steel or rhenium gasket hole in the diamond cell sample chamber, sandwiched between two $\sim5-10$ μm layers of either MgO, NaCl, or Al_2O_3. These layers provide a thermal barrier between the sample and the diamond surfaces, and also serve as an independent pressure calibrant, albeit one that experiences a different range of temperatures than the sample mixture.

Energy-dispersive x-ray diffraction experiments were performed at X17B1 of the National Synchrotron Light Source at Brookhaven National Laboratory, and the GSECARS sector of the Advanced Photon Source. Collimating slits were employed to form an approximately 10×10 μm x-ray beam, and the diffracted energy was collected with a solid state detector at $2\theta=8°-10°$. The detector was calibrated with a series of fluorescence standards, and the angle was calibrated using a gold foil. Details of the two-circle energy dispersive diffractometer system can be found elsewhere.[28]

The sample was heated simultaneously on both sides using a Nd:YLF laser.[29,30] To measure the temperature, spectral intensity of thermal radiation was measured as a function of distance across the hotspot imaged through a vertical slit using an imaging spectrometer and charge coupled device. The temperature on each side was determined by fitting the spectral intensity data, corrected for system response determined by a standard tungsten lamp (Optronics Co.) traceable

TABLE I. Laser heating experimental conditions.

Name	Sample	Insulating medium	Pressure range (GPa)
N62A	Pt+MgO	NaCl	24–40
N62B	Pt+MgO	NaCl	15–48
N63A	Pt+MgO	Al_2O_3	35–63
N63B	Pt+MgO	Al_2O_3	25–50
A8A	Pt+NaCl	MgO	23–32
A8B	Pt+NaCl	MgO	14–24
A8C	Pt+NaCl	MgO	16–22
A8D	Pt+NaCl	MgO	20–22

to the National Institute of Standards and Technology, to a graybody spectrum at each point across the hotspot image.[3] Temperatures reported for each diffraction pattern are from the peak intensities at the center of the hotspot.

During a thermal cycle, the laser power was typically slowly (~1 min) increased, held constant for several minutes, and slowly lowered (~1 min). X-ray diffraction patterns were collected throughout the heating cycle, with patterns obtained before, during (at $\sim1-2$ min intervals), and after heating. Corresponding temperature measurements from each side of the sample and x-ray diffraction patterns were obtained at ~1 min intervals throughout the course of each temperature cycle, for a total of about 20 diffraction patterns and temperature profiles over 20–30 min. In some cases, a temperature cycle was repeated on the same sample at the same pressure at the same spot or a previously unheated spot; in other cases, the pressure was increased and a new heating cycle began. A summary of the heating cycle experiments is shown in Table I.

EXPERIMENTAL RESULTS

Representative x-ray diffraction patterns from two heating cycles are shown in Fig. 2. The $P(V,T)$ paths traced out by platinum in the laser heated diamond cell for these experiments (Fig. 3) show significant deviations from the ideal behavior (Fig. 1). To determine the pressure contours in Figs. 1, 3, and 4, the equation of state is written as a sum of the room-temperature equation of state and a thermal pressure term P_{th}[31]
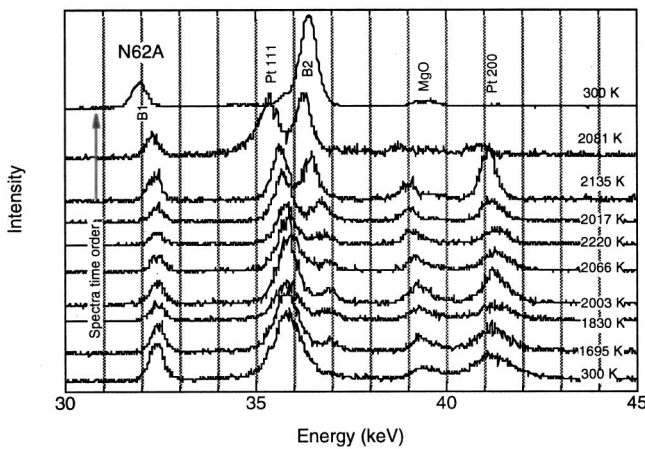
$$P(V,T)=P(V,300)+P_{th}, \qquad (1)$$

where T is the sample temperature. The third order Birch–Murnaghan equation is used to determine $P(V,300\,\text{K})$. We adopt a simple form for P_{th}, which assumes that αK_T is independent of volume and temperature[31]
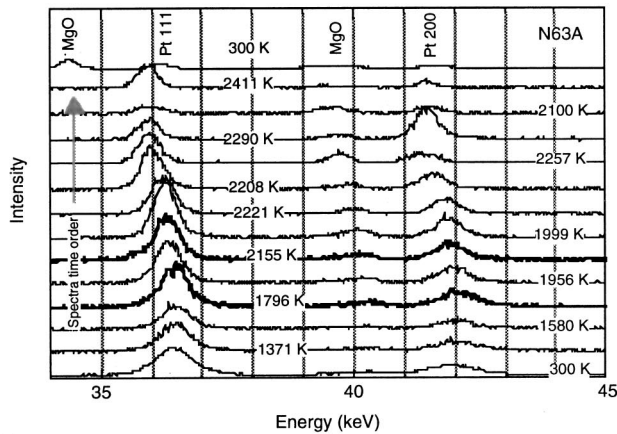
$$P_{th}=\alpha_0 K_{T0}(T-300), \qquad (2)$$

where α is the volume thermal expansivity, K_T is the isothermal bulk modulus, and the subscript 0 refers to ambient pressure conditions. High-temperature elastic moduli and thermal expansion data indicate that the product $\alpha_0 K_{0T}$ is largely independent of temperature up to ~1800 K for platinum.[32,33] Equation of state parameters for platinum and MgO are shown in Table II.

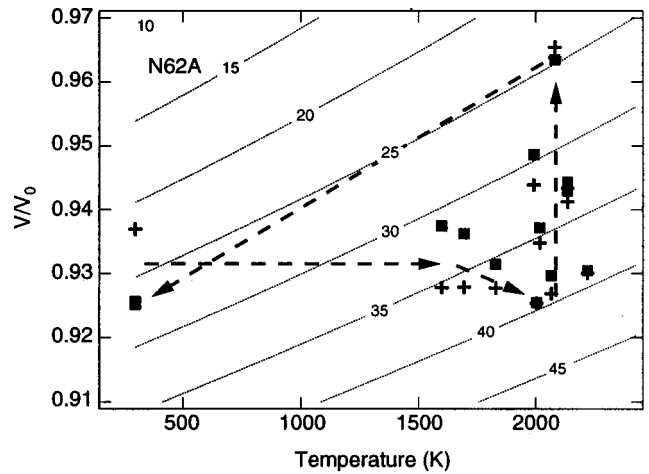The results in Fig. 3 show that complexity in the observed paths was the rule, rather than the exception, with
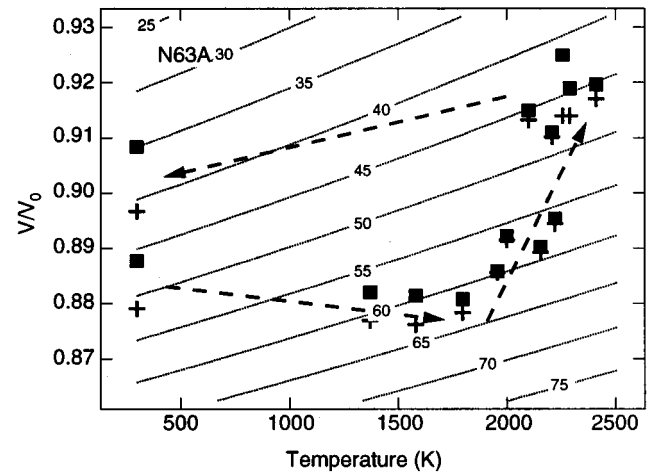
FIG. 2. Representative energy-dispersive x-ray diffraction patterns recorded using $2\theta=9.001(5)$. The temperatures next to each pattern are the hotspot center temperatures recorded on the upstream side (toward the x-ray source) of the sample. The time order of the spectra is bottom to top, denoted by the arrow. Pt, MgO, and NaCl B1 and B2 diffraction peaks are labeled. (a) N62A and (b) N63A.

only A8C [Fig. 3(d)] and A8D (not shown) demonstrating reversible (but not constant pressure) paths. The path results display a wide variety of behavior that may be dependent on differences in sample preparation and loading, gasket material, pressure medium, and perhaps the design of the diamond cell itself. However, there are some fundamental observations applicable to all of the measurements.
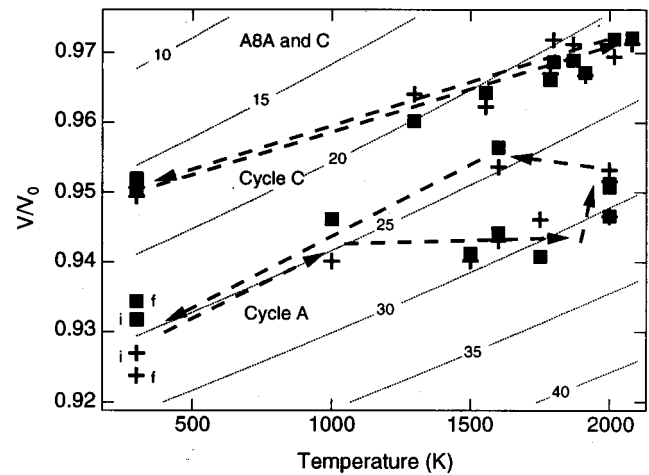
The first general observation is that the environment inside the sample chamber does not remain at constant pressure during heating, consistent with previous *in situ* experiments and theoretical calculations.[4–7] For example, the pressure determined from platinum in path N62A [Fig. 3(a)] starts at ~24 GPa before heating, increases to 40 GPa at a temperature of 2100 K, and then drops from 40 to 25 GPa as the temperature is maintained. Path N63A [Fig. 3(b)] demonstrates similar behavior, with preheating volumes indicating pressures of ~50 GPa, increasing to 63 GPa during heating to 1800 K. There is also a large pressure drop to less than 45 GPa, as the temperature is held at ~2000 K. Except for samples that had already experienced several temperature cycles at the same compression, every measured path showed this pressure relaxation at high temperatures. In

FIG. 3. Volume vs temperature paths for platinum obtained from diffraction data. Relative compression is determined independently from the 111 (+) and 200 (■) lattice reflections and plotted as a function of peak hotspot temperature. Arrows show the progression of the heating cycle. Where necessary, preheat and quench values are denoted by i and f, respectively. The contours show pressures (in GPa) determined from the platinum equation of state (Table II). (a) N62A, (b) N63A, and (c) A8A and A8C.

many cases the apparent initial pressure increase and/or the observed pressure drop at high temperatures is greater than the thermodynamically allowed limit given by the thermal pressure [Eq. (1); Fig. 1]. In the case where both Pt and MgO
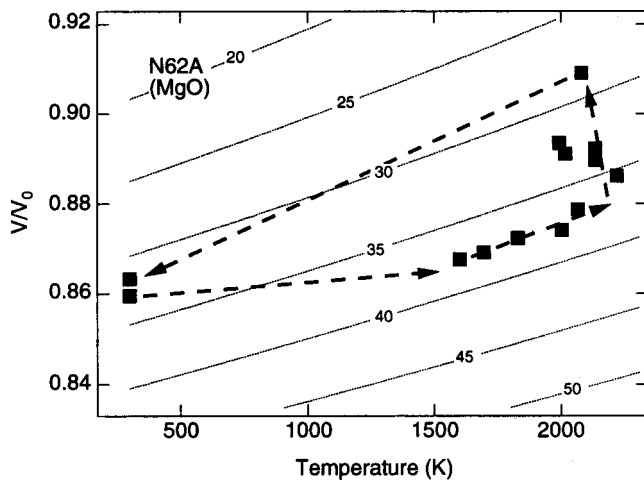
FIG. 4. Volume vs temperature path for MgO determined from its (200) reflection during cycle N62A [cf. Fig. 3(a)]. The contours show pressures (in GPa) determined from the MgO equation of state (Table II).

are mixed together within the sample chamber, both markers indicate a qualitatively similar path [Figs. 3(a) and 4].

Another fundamental observation is that the volumes measured before and after heating are not reliable indicators of the pressure at high temperature. For example, despite the large pressure changes experienced by the cycle depicted in Fig. 3(a), the pressure determined by the measured d spacing of Pt before and after heating are within 2–3 GPa of 25 GPa. Figure 3(b) also demonstrates that the volume measurements before and after heating do not reflect the pressure changes at high temperatures because of significant differences in the heating and cooling paths. In this case, the pressure change recorded by comparing volumes before and after heating, ~10 GPa, is 50% lower than the 20 GPa drop observed while the sample is held at ~2000 K.

A close look at the diffraction data for these temperature cycles reveals that the (200) reflection of Pt yields systematically higher lattice parameters than the (111) line, especially at room temperature, and during the first few diffraction patterns of a heating cycle [e.g., Figs. 3(a)–3(c)]. This

TABLE II. Equation of state parameters for Pt and MgO. V_0 is the ambient-pressure unit cell volume; K_{0T} is the isothermal bulk modulus and K'_{0T} its pressure derivative. α_0 is the room-temperature volume thermal expansion coefficient. The S_{ij}'s are the elastic compliances at ambient conditions, and S'_{ij} is the corresponding pressure derivative.

	Pt	MgO
V_0 (Å^3)	60.3793[a]	74.6716
K_{0T} (GPa)	278[a]	160.3[c]
K'_{0T}	5.6[a]	4.1[c]
α_0 (K^{-1})	$26.8 \times 10^{-6,a}$	$31.6 \times 10^{-6,e}$
$S_{11} - S_{12}$ (GPa^{-1})	0.010 42[b]	
$(S_{11} - S_{12})'$ (GPa^{-2})	−0.000 08[d]	
S_{44} (GPa^{-1})	0.013 66[b]	
S'_{44} (GPa^{-2})	−0.000 20[b]	

[a]Reference 44.
[b]References 35 and 36.
[c]Reference 45.
[d]Estimated based on elasticity systematics of fcc metals (Ref. 37).
[e]Reference 46.

difference can be interpreted using lattice strain theory[9] as the result of platinum's elastic anisotropy and the existence of deviatoric stress. This significantly affects the interpretation of the apparent paths, and will be developed further in the next section.

The final general observation from our data indicates that thermal cycling of the same spot may decrease the hysteresis effect at high temperatures [Fig. 3(c)]. In fact, the only measured paths that showed quasireversible paths were for samples that had been through several previous heating cycles at the same spot on the sample. These cycles follow a quasireversible path that can be interpreted within the constant pressure-constant volume continuum. A comparison of the platinum measurements in cycle A8C with the contours established by its equation of state, shows that if thermal pressure was not taken into account, the platinum data would yield a thermal expansion lower than expected. This is consistent with previous results for MgO in the laser-heated diamond anvil cell.[5]

The accuracy of the temperature measurement plays a large role in our ability to deconvolve thermal expansion and thermal pressure effects.[17] Because we measure large temperature gradients (~30–60 K/μm) across the area of the x-ray beam in these experiments, the temperature at the hotspot center is an upper bound on the actual average temperature of the x-rayed volume, which can be 200–500 K lower. Misalignments between the x-ray and laser beam profiles will further contribute to a similar error in temperature measurement.[17] The magnitude of these errors is dependent on the steepness of the temperature gradient and the amount of misalignment, both of which may vary considerably from experiment to experiment. Because these errors yield a systematic overestimation of the temperature, the result is to move all of the high-temperature data points in Figs. 3 and 4 to the left. If the true temperatures are systematically lower, then the true thermal expansion should tend to be higher and the true thermal pressure terms should tend to be lower, resulting in a strong effect on thermal expansion and thermal pressure calculations.[17] However, our qualitative interpretation of the measured paths remains undisturbed by a systematic error in temperature. Indeed, the observations of large pressure drops at high temperatures requires that those temperatures be underestimated by thousands of degrees in order to be able to account for that behavior using thermal pressure/thermal expansion arguments.

Additional systematic errors in the temperature measurement include the effects of a temperature or wavelength-dependent emissivity and errors contributed by the system response calibration and optical aberrations. Of these, the wavelength-dependent emissivity is the largest contributor to the temperature error, estimated to be ~200 K for Pt.[34] In addition to errors in accuracy, the precision of each temperature measurement is affected by fluctuations of the hotspot center about the x-ray beam, temporal fluctuations in temperature due to changes in laser power and hotspot–laser coupling, and noise in the spectroradiometry data and in the calibration curves. These errors are estimated to be ~50–100 K;[17,18] not enough to have a significant effect on the results.

MODEL DESCRIPTION

To aid in analyzing the experimental results, we developed a model to calculate the positions of platinum diffraction peaks as a function of temperature and stress state within the diamond cell. By generalizing the $P(V,T)$ equation of state [Eq. (1)] to a $\sigma(\epsilon,T)$ (stress–strain) equation of state, we can include the effects of deviatoric stress

$$\sigma(\epsilon_{\text{meas}}T) = \sigma_{\text{hydro}}(\epsilon_{\text{hydro}},300) + \sigma_{\text{hydro},th}(\epsilon_{\text{hydro},th},T)$$
$$+ \sigma_{\text{dev}}(\epsilon_{\text{dev}}(hkl),300), \qquad (3)$$

where σ and ϵ are the stress and strain tensors, and the subscript meas refers to the strains measured by x-ray diffraction line positions. The subscripts hydro and dev refer to the hydrostatic and deviatoric components, and the subscript th refers to the temperature-dependent stress and strain terms. We assume that there are no deviatoric stresses at high temperatures, as discussed below. The hydrostatic component of the stress tensor [the first two terms on the right-hand side of Eq. (3)] is given by Eqs. (1) and (2). The equation describing $\epsilon_{\text{dev}}(hkl)$ for a cubic material in the diamond anvil cell x-ray geometry is[9]

$$\epsilon_{\text{dev}}(hkl) = (t/3)(S_{11} - S_{12} - 3S\Gamma(hkl))(1 - 3\cos^2\psi), \qquad (4)$$

where t is the differential stress being supported by the sample, and equal to $\sigma_1 - \sigma_3$, where σ_1 is the axial stress and σ_3 is the radial stress; Sij are the single-crystal elastic compliances; S is defined as $S_{11} - S_{12} - 0.5S_{44}$; ψ is the angle between the principal stress direction and the diffracting plane normal, and $\Gamma(hkl)$ is a geometric factor given by $(h^2k^2 + k^2l^2 + h^2l^2)/(h^2 + k^2 + l^2)^2$. Equation (4) describes how each diffraction line of a cubic material is shifted from its hydrostatic value in response to an additional deviatoric stress and encompasses two effects: (1) all lines shift to lower energies (higher d spacing), by an amount proportional to $S_{11} - S_{12}$; and (2) each (hkl) may experience a slightly different additional shift, depending on the magnitude of S. If $S > 0$, the (200) line will yield a higher d spacing than the (111) line; if $S < 0$, the converse is true. The elastic moduli of platinum and their pressure dependencies are taken from existing data and systematics of face centered cubic (fcc) metals.[35–37]

The presence of deviatoric stress, if unrecognized, can introduce a significant error in the pressure determination (Fig. 5). For example, for platinum under hydrostatic conditions at 30 GPa, a differential stress of 2 GPa[14,26,32,38] will increase the average volume recorded by the (111) (200) and (220) lines by 0.7%. If it is assumed that this corresponds to the volume strain under hydrostatic pressure, the calculated pressure would be 26.7 GPa, an underestimate of 11% (Fig. 5). In addition, platinum's elastic anisotropy also will cause each diffraction line to yield a slightly different lattice parameter value. The small standard error due to this effect is $\Delta V/V = 0.2\%$, close to the detection limit for energy-dispersive x-ray diffraction measurements.
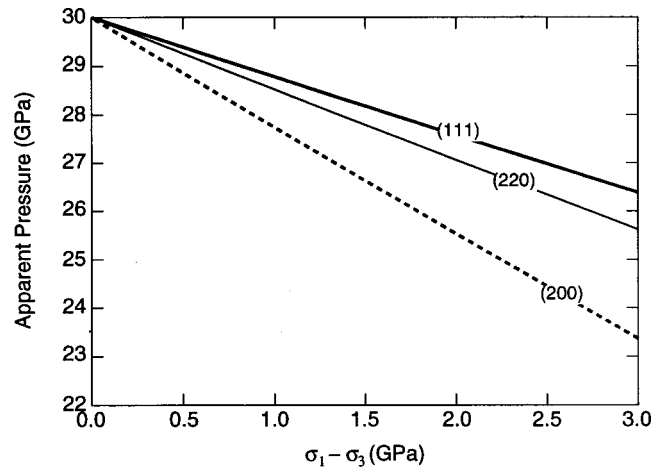

FIG. 5. The apparent pressure determined by assuming the measured d spacing for the (111), (200), and (220) diffraction lines of platinum correspond to the volume strain under hydrostatic pressure, as a function of differential stress, $(\sigma_1 - \sigma_3)$. The hydrostatic pressure is 30 GPa.

INTERPRETATION OF $P(V,T)$ PATHS DURING LASER HEATING

This model allows us to calculate $P(V,T)$ paths for platinum as a function of hydrostatic pressure, deviatoric stress, and temperature. For example, Fig. 6 shows a constant pressure path (30 GPa) with an initial differential stress (3 GPa) that decreases during heating to show qualitatively the effect of annealing a shear stress. This path yields an apparent large increase in pressure resulting from the annealing of differential stress at high temperature, similar to what is observed during initial heating in many of our measured paths [Figs. 3(a) and 3(b)]. Otherwise, the simulation bears little resemblance to our measured paths.

The (111) and (200) reflections for Pt provide a unique determination of both the hydrostatic and shear components of the stress tensor if the elastic moduli are known as a
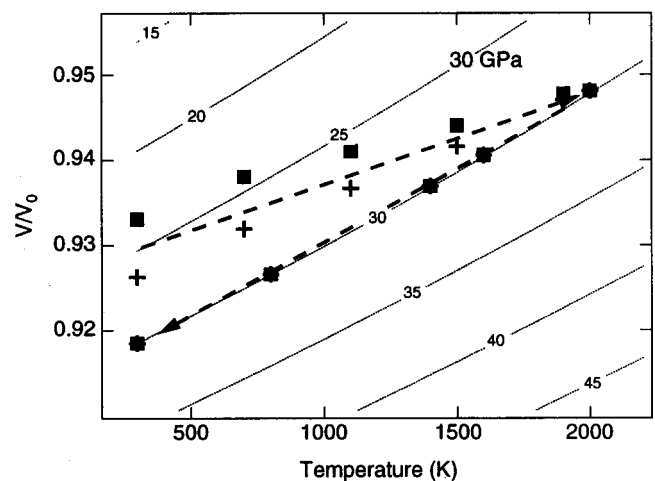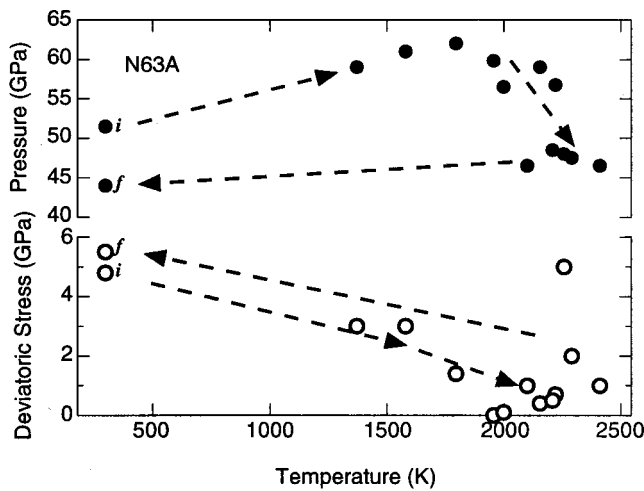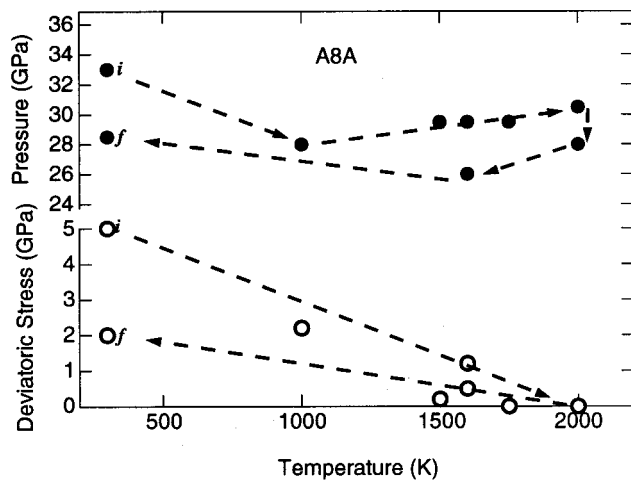

FIG. 6. Volumes calculated for platinum in a laser-heated diamond cell under constant pressure (30 GPa) conditions, with a relaxation of an initial 3 GPa differential stress during heating. Compressions calculated for the (111) (+) and (200) (■) reflections are plotted as a function of temperature. Arrows show the time evolution of the heating cycle. Contours are the same as for Figs. 1 and 3.

(a)

(b)

FIG. 7. The hydrostatic and deviatoric components of the stress tensor deconvolved for (a) N63A and (b) A8A (cf. Fig. 3). Arrows show the time sequence of the heating cycle.
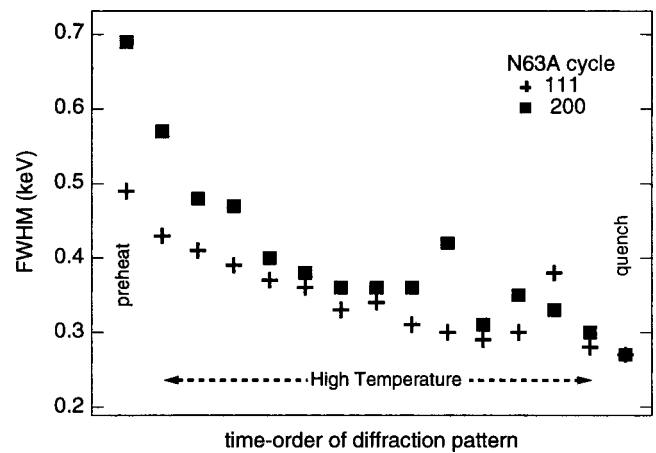

FIG. 8. Platinum diffraction line width for N63A. The FWHM of platinum diffraction lines (111) (+) and (200) (■) plotted in order of measurement.

function of pressure and temperature. We can thus use our model in an inverse fashion to deconstruct the hydrostatic and shear components of the stress tensor from our measurements throughout the heating cycle. For each diffraction pattern, ϵ_{111} and ϵ_{200} are calculated from the positions of platinum lattice reflections. The deviatoric stress is calculated from the difference $\epsilon_{111} - \epsilon_{200}$ through Eq. (4). The hydrostatic stress is then calculated using Eq. (3). Results of these calculations for paths N63A and A8A (Figs. 3(b) and 3(c)) are shown in Figs. 7(a) and 7(b). Figure 7 shows that when deviatoric stresses are accounted for, the magnitude of the initial pressure increase during heating is much reduced or even reversed in sign.

In general, metals at high temperature are not expected to support significant amounts of shear stress. Our observations support this, showing that deviatoric stresses relax during heating, and are small at high temperatures (Fig. 7). This is consistent with independent measurements of the relaxation of shear stresses during heating in the diamond cell,[11] as well as results from multianvil press experiments.[39]

Interestingly, our observations suggest that deviatoric stresses can be reintroduced into the sample upon thermal quench. For example, Figs. 7(a) and 7(b) show an initial shear stress of approximately 5 GPa that reduces to near 0 during heating. Upon quench, varying amounts of shear stress may be reintroduced. This is consistent with observations during laser heating in a diamond cell of a Pt–CaSiO$_3$ mixture,[14] but inconsistent with observations of heating in a large-volume press.[13] We speculate that this deviatoric stress arises from mechanical stresses introduced to gasket, sample, and/or cell during the rapid thermal quench when the laser is shut off. However, our results also show evidence [Figs. 3(c) and 3(d)] that the shear stresses, including those reintroduced during quench, are reduced after the sample undergoes several thermal cycles.

The discussion on shear stress has so far been limited to the macroscopic scale. However, because our samples start as loose powders and are compressed to high pressures at low temperatures, they are subjected to significant amounts of shear stress localized at the particle boundaries. Microscopic shear stresses increase the diffraction line width because each diffracting crystallite is subjected to a different localized stress condition. The full width at half maximum (FWHM) of the diffraction lines, and their change during heating, can therefore be an indicator of the extent of localized shear strains within the individual grains of the sample. Figure 8 shows that our results are consistent with previous results on the annealing of microscopic shear stresses[39] with temperature at high pressure. The fact that Fig. 7 shows shear stresses present after quenching despite no evidence of line broadening underscores the distinction between the macroscopic deviatoric stress experienced by the sample as a whole, and local deviatoric stresses present on a microscopic scale.

The above analysis rests on the assumption that all of the diffraction peaks in a single record reflect the d spacing of platinum at a single pressure and temperature (or a time- and x-ray volume-average of pressure and temperature). This may not be the case if we consider the possibility of recrystallization, growth, and texturing in a background of tem-
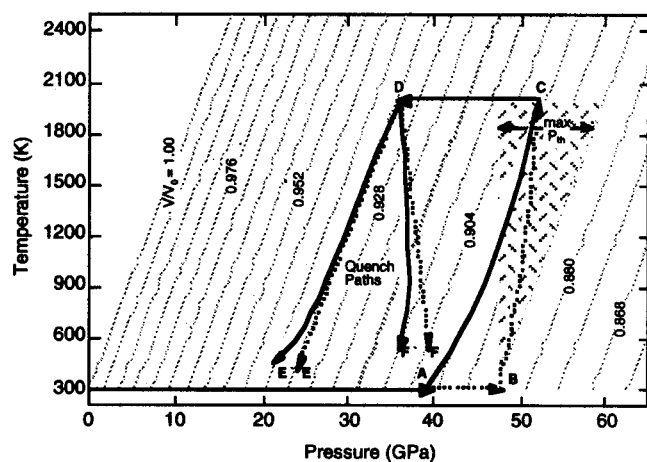
FIG. 9. A schematic illustration depicting the possible paths followed by a platinum pressure marker in the laser-heated diamond cell. The constant-volume contours depict the equation of state of Pt.[44] The dashed lines show the actual P,T path traveled by the platinum marker, and the solid lines show the path that would be measured in the presence of a deviatoric shear stress t_i which relaxes during heating. The shaded area depicts the boundary between constant volume and constant pressure conditions during heating, and the maximum allowable thermal pressure is shown.

perature and pressure fluctuations. For example, if the intensity of the (111) peak of platinum represents a true powder diffraction average over time (say $V/V_0 = 0.96$, corresponding to 1500 K and 30 GPa), but most of the intensity of the (200) diffraction peak is contributed by a single crystallite that fleetingly satisfied Bragg's law at the same pressure but at 2000 K, the (200) line will yield a V/V_0 of 0.97. This difference, if interpreted based on our model, would imply a deviatoric stress of 3 GPa. Texturing, however, is not our preferred interpretation, because it predicts random differences between (111) and (200) positions, unlike the systematically lower (111) d spacing that we observe. In addition, if texturing were a significant problem, we would expect that each of our measured diffraction patterns would show widely varying relative intensities for the diffraction lines of each material. Figure 2 shows, however, that the relative intensities of the (111) and (200) lines remain approximately constant, and consistent with predicted values. On the other hand, the presence of texturing may contribute some noise to the signal, yielding errors in the quantitative (but not qualitative) interpretation of the paths.

Neither thermal pressure nor deviatoric stress can explain the large-scale pressure relaxation observed at ~2000 K. We speculate that these arise from the effects of heating of components of the cell outside the x-rayed volume, such as the pressure medium, gasket, and even the body of the cell itself. Pressure relaxations of this sort have been previously reported in the externally heated diamond cell where the pressure was found to decrease by ~1 GPa for every 20 K of temperature increase to the cell,[40] with qualitatively similar observations in multianvil experiments.[41]

SUMMARY

Figure 9 shows a schematic of the processes that may occur during laser heating in a diamond anvil cell, and their effect on the pressure measurement using a platinum standard. At room temperature, the apparent pressure (point A in Fig. 9) is less than the true hydrostatic pressure (point B). During heating, as deviatoric stresses are annealed, there may be an apparent pressure increase (path AC) in addition to the change in hydrostatic pressure (Path BC). At high temperatures, large-scale pressure relaxation may occur (CD). Finally, during quench, the sample environment can vary considerably, including constant pressure, constant volume (DE), and pressure-inducing paths (DF). Deviatoric stress (DE' and DF') may be introduced during thermal quench, which lower the apparent pressure.

In Heinz's model of thermal pressure,[4] pressure differences are observed by comparing volume measurements made before and after the heating cycle. For the case where only thermal pressure and thermal expansion in an elastic medium are considered, the maximum pressure change possible is thermodynamically limited to $\alpha K \Delta T$, which is equal to 12.5 GPa for platinum heated to 2000 K. Therefore, the "equilibrium effects" of thermal pressure and thermal expansion alone (Fig. 1) cannot be responsible for many of the path observations (Fig. 7). This effect is not predicted by more recent models of the sample during laser heating based on thermal pressure considerations,[7] however, large changes of pressure have been observed before and after heating in other experiments.[41,42] The possibility of pressure changes outside the boundary delineated by thermal pressure has significant implications for much work done on materials at high P and T in the diamond anvil cell. Many of these experiments, where pressure is not monitored in situ, use pressures measured both before and after heating as proxies for the pressures at high temperatures.[34,43] Our results clearly underscore the necessity of including an in situ pressure tracer during heating experiments.

By comparing measured $P(V,T)$ paths within the laser-heated diamond cell with results from calculations designed to simulate the behavior of a sample during heating, we can explain the observed behavior of a sample during heating, and determine the criteria for making an accurate equation of state measurement at high temperatures and pressures. At least four distinct processes occur within the sample chamber during laser heating that may cause the sample environment to deviate from the ideal constant pressure case. The first is the thermal pressure effect, resulting from a sample environment with volume constrained during heating. Second, deviatoric stresses can exist within the sample chamber, which can cause large underestimates of the pressure before and after heating, and large apparent pressure increases during heating. Deviatoric stresses can be present at both the macroscopic and microscopic level. Each of these deviatoric stress effects is reduced during heating, but only the reduction in microscopic deviatoric stress is maintained on thermal quench. Finally, at the elevated temperatures reached during laser heating, there are large scale pressure variations, usually relaxation, that change the hydrostatic pressure by amounts beyond that allowed by the thermal pressure. These are often not recovered in the quenched sample, making imperative the use of in situ stress markers during laser heating experiments.

ACKNOWLEDGMENTS

[1] H. K. Mao, P. M. Bell, J. W. Shaner, and K. J. Steinberg, J. Appl. Phys. **49**, 3276 (1978).

[2] C. Jamieson, J. N. Fritz, M. H. Manghnani, in *High Pressure Research in Geophysics*, edited by S. Akimoto and M. Manghnani (Reidel, Boston, MA, 1982), pp. 27–48.

[3] D. L. Heinz and R. Jeanloz, in *High Pressure Research in Mineral Physics*, edited by M. Manghnani and Y. Syono (American Geophysical Union, Washington DC, 1987), p. 113.

[4] D. L. Heinz, Geophys. Res. Lett. **17**, 1161 (1990).

[5] G. Fiquet, D. Andrault, J. P. Itie, P. Gillet, and P. Richet, Phys. Earth Planet. Inter. **95**, 1 (1996).

[6] D. Andrault, D. G. Fiquet, J. P. Itie, P. Richet, P. Gillet, D. Hausermann, and D. M. Hanfland, Eur. J. Mineral. **10**, 931 (1998).

[7] A. Dewaele, G. Fiquet, and P. Gillet, Rev. Sci. Instrum. **69**, 2421 (1998).

[8] G. L. Kinsland, High Temp.-High Press. **10**, 627 (1978).

[9] A. K. Singh, J. Appl. Phys. **73**, 4278 (1993).

[10] T. S. Duffy, R. J. Hemley, and H. K. Mao, Phys. Rev. Lett. **74**, 1371 (1995).

[11] Y. Meng and D. J. Weidner, Geophys. Res. Lett. **20**, 1147 (1993).

[12] T. S. Duffy and Y. Wang, in *Ultrahigh-Pressure Mineralogy*, edited by R. J. Hemley (Mineralogical Society of America, Washington DC, 1998), pp. 426–457.

[13] D. J. Weidner *et al.*, in *High Pressure Research: Applications to Earth and Planetary Sciences*, edited by Y. Syono and M. H. Manghnani (American Geophysical Union, Washington DC, 1992), pp. 13–17.

[14] S. H. Shim, T. S. Duffy, and G. Shen, Phys. Earth Planet. Inter. **20**, 327 (2000).

[15] R. Boehler, N. von Bargen, and A. Chopelas, J. Geophys. Res. B **95**, 21731 (1990).

[16] Q. Williams, E. Knittle, and R. Jeanloz, J. Geophys. Res. B **96**, 2171 (1991).

[17] A. Kavner, Rev. Sci. Instrum. (submitted).

[18] A. Kavner and W. Panero (unpublished).

[19] S. Saxena *et al.*, Science **274**, 1357 (1996).

[20] G. Serghiou, A. Zerr, and R. Boehler, Science **280**, 2093 (1998).

[21] L. Dubrovinsky *et al.*, Science **285**, 983 (1999).

[22] G. Fiquet, A. Dewaele, D. Andrault, M. Kunz, and T. Le Bihan, Geophys. Res. Lett. **27**, 21 (2000).

[23] R. Serghiou, A. Zerr, L. Chudinovskikh, and R. Boehler, Geophys. Res. Lett. **22**, 441 (1995).

[24] J. Zhang, B. Li, W. Utsumi, and R. C. Libermann, Phys. Chem. Miner. **23**, 1 (1996).

[25] J. Liu, L. Topor, J. Zhang, A. Navrotsky, and R. C. Liebermann, Phys. Chem. Miner. **23**, 11 (1996).

[26] A. Dewaele, G. Fiquet, D. Andrault, and D. Hausermann, J. Geophys. Res. B **105**, 2869 (2000).

[27] S. H. Shim, T. S. Duffy, and G. Shen, J. Geophys. Res. B **105**, 25 955 (2000).

[28] M. L. Rivers, T. S. Duffy, Y. Wang, P. J. Eng, S. R. Sutton, and G. Shen, in *Properties of Earth and Planetary Materials at High Pressure and Temperature*, edited by M. H. Mangnhnani and T. Yagi (AGU, Washington DC, 1998), pp. 79–87.

[29] H. K. Mao, G. Shen, R. J. Hemley, and T. S. Duffy, in *Properties of Earth and Planetary Materials at High Pressure and Temperature*, edited by M. H. Mangnhnani and T. Yagi (AGU, Washington DC, 1998), Vol. 101, pp. 27–34.

[30] G. Shen, H. K. Mao, and R. J. Hemley, in *Proceedings of the Third NIRIM International Symposium on Advanced Materials, March 4–8, Tokyo, Japan*, 1996, pp. 149–152.

[31] O. Anderson, *Equations of State of Solids for Geophysics and Ceramic Science* (Oxford University Press, New York, 1995).

[32] T. S. Duffy, A. Kavner, and S. Shim, American Geophysical Union Spring Meeting Conference, May 30–June 3, Washington, DC.

[33] S. M. Collard and R. B. McLellan, Acta Metall. Mater. **40**, 699 (1992).

[34] A. Kavner and R. Jeanloz, J. Appl. Phys. **83**, 7553 (1998).

[35] R. E. MacFarlane, J. A. Rayne, and C. K. Jones, Phys. Lett. **18**, 91 (1965).

[36] S. N. Biswas, M. J. P. Muringer, and C. A. Ten Seldam, Phys. Status Solidi A **141**, 361 (1994).

[37] G. Simmons and H. Wang, *Single Crystal Elastic Constants and Calculated Aggregate Properties, A Handbook* (MIT, London, 1971), p. 370.

[38] *Metals Handbook*, 10th edition (ASM International, Materials Park, OH, 1990), Vol. 2.

[39] D. J. Weidner, Y. Wang, and M. T. Vaughan, Geophys. Res. Lett. **21**, 753 (1994).

[40] Y. Fei, H.-k. Mao, J. Shu, and J. Hu, Phys. Chem. Miner. **18**, 416 (1992).

[41] K. Kuroda, T. Irifune, T. Inoue, N. Nishiyama, M. Miyashita, K. Funakoshi, and W. Utsumi, Phys. Chem. Miner. **27**, 523 (2000).

[42] Y. Tsuchida and T. Yagi, Nature (London) **340**, 217 (1989).

[43] A. Zerr, G. Serghiou, and R. Boehler, Geophys. Res. Lett. **24**, 909 (1997).

[44] N. C. Holmes, J. A. Moriarty, G. R. Gathers, and W. J. Nellis, J. Appl. Phys. **66**, 2962 (1989).

[45] D. G. Isaak, O. L. Anderson, and T. Goto, Phys. Chem. Miner. **16**, 704 (1989).

[46] I. Suzuki, J. Phys. Earth **23**, 145 (1975).